# Specific Hydrogen-Bonding Networks Responsible for Selective $O_2$ Sensing of the Oxygen Sensor Protein HemAT from *Bacillus subtilis*†

Hideaki Yoshimura,‡,§ Shiro Yoshioka,‡ Katsuaki Kobayashi,‡ Takehiro Ohta,‡,|| Takeshi Uchida,‡,⊥ Minoru Kubo,‡ Teizo Kitagawa,‡ and Shigetoshi Aono*,‡

*Okazaki Institute for Integrative Bioscience, National Institutes of Natural Sciences, 5-1 Higashiyama, Myodaiji, Okazaki, Aichi 444-8787, Japan, and The Department of Structural Molecular Science, School of Physical Sciences, The Graduate University for Advanced Studies, 38 Nishigonaka, Myodaiji, Okazaki, Aichi 444-8585, Japan*

*Received February 15, 2006; Revised Manuscript Received May 18, 2006*

ABSTRACT: HemAT from *Bacillus subtilis* (HemAT-*Bs*) is a heme-based $O_2$ sensor protein that acts as a signal transducer responsible for aerotaxis. HemAT-*Bs* discriminates its physiological effector, $O_2$, from other gas molecules to generate the aerotactic signal, but the detailed mechanism of the selective $O_2$ sensing is not obvious. In this study, we measured electronic absorption, electron paramagnetic resonance (EPR), and resonance Raman spectra of HemAT-*Bs* to elucidate the mechanism of selective $O_2$ sensing by HemAT-*Bs*. Resonance Raman spectroscopy revealed the presence of a hydrogen bond between His86 and the heme propionate only in the $O_2$-bound form, in addition to that between Thr95 and the heme-bound $O_2$. The disruption of this hydrogen bond by the mutation of His86 caused the disappearance of a conformer with a direct hydrogen bond between Thr95 and the heme-bound $O_2$ that is present in WT HemAT-*Bs*. On the basis of these results, we propose a model for selective $O_2$ sensing by HemAT-*Bs* as follows. The formation of the hydrogen bond between His86 and the heme propionate induces a conformational change of the CE-loop and the E-helix by which Thr95 is located at the proper position to form the hydrogen bond with the heme-bound $O_2$. This stepwise conformational change would be essential to selective $O_2$ sensing and signal transduction by HemAT-*Bs*.

Diatomic gas molecules such as dioxygen ($O_2$[1]), carbon monoxide (CO), and nitric oxide (NO) can work as signaling molecules with the cognate receptor proteins in biological systems. The heme-based sensor proteins are the most general receptor proteins for these gas molecules (*1*−*3*). The heme in these proteins functions as the binding site for their effector gas molecules. These heme-based gas sensor proteins must discriminate the effector from other molecules so as to take a specific conformation only upon the binding of the effector molecule. However, the discrimination of these gas molecules is difficult for heme proteins because $O_2$, CO, and NO have similar size and can be bound to a reduced heme with a similar coordination structure. The ligand discrimination mechanism of the heme-based gas sensor proteins is not fully understood yet.

HemAT is a heme-based $O_2$ sensor protein that functions as a signal transducer for bacterial aerotaxis (*4*−*7*). The HemAT monomer consists of two domains, a sensor domain and a signaling domain. The sensor domain shows a globin fold containing a heme that acts as the $O_2$ binding site. The signaling domain of HemAT interacts with a histidine kinase protein CheA, a component of the CheA/CheY two-component signal transduction system that regulates the direction of the flagellar motor rotation (*8*−*10*).

A specific conformational change of HemAT will occur around the heme upon $O_2$ binding, and then intramolecular signal transduction takes place from the sensor domain to the signaling domain. As a result, the self-kinase activity of CheA is regulated by a change in the HemAT−CheA interaction via the conformational change of HemAT. This signaling event takes place only with $O_2$ but not with other gas molecules. However, the detailed mechanisms of selective $O_2$ sensing and signal transduction of HemAT remain to be elucidated.

To elucidate these mechanisms of HemAT, it is necessary to characterize the heme environmental structure, including the coordination structure of the heme and the hydrogen-bonding pattern around the heme and the ligand. The crystal structure of the sensor domain of HemAT from *Bacillus subtilis* (HemAT-*Bs*) reveals that Tyr70 and Thr95 in the distal heme pocket are possible candidates of amino acid residues for forming hydrogen bonds with the heme-bound ligand (*11*) (Figure 1). Resonance Raman spectroscopy has revealed that Thr95 forms hydrogen bonds to the heme-bound $O_2$, which gives two different conformers, and that

† This work was supported by a Grant-in-Aid for Scientific Research on Priority Areas (Chemistry of Coordination Space) (17036072 to S.A.) and a Grant-in-Aid for Young Scientists B (17770118 to S.Y.) from the Ministry of Education, Culture, Sports, Science, and Technology, Japan and by a Grant-in-Aid for Scientific Research B (16370065 to S.A.) from the Japan Society for the Promotion of Science.

* To whom correspondence should be addressed: Tel: +81 564 59-5575. Fax: +81 564 59-5576. E-mail: aono@ims.ac.jp.

‡ National Institutes of Natural Sciences.

§ The Graduate University for Advanced Studies.

|| Present address: Department of Chemistry, Stanford University, 333 Campus Drive, Stanford, CA 94305-5080.

⊥ Present address: Division of Chemistry, Graduate School of Science, Hokkaido University, Kita 10, Nishi 8, Kita-ku, Sapporo 060-0810, Japan.

[1] Abbreviations: CO, carbon monoxide; EPR, electron paramagnetic resonance; HemAT-*Bs*, the full-length HemAT from *Bacillus subtilis*; Mb, myoglobin; NO, nitric oxide; $O_2$, dioxygen; WT, wild type.

10.1021/bi060315c CCC: $33.50 
Published on Web 06/21/2006

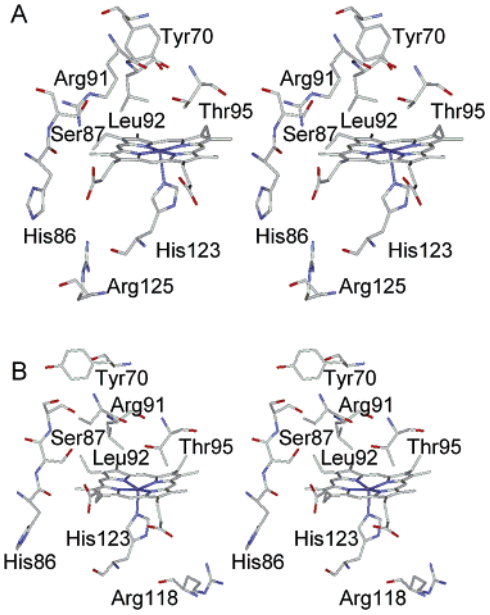


FIGURE 1: Stereoviews of the heme environmental structures of deoxy HemAT-*Bs*; (A) subunit A and (B) subunit B (pdb 1OR6) (*9*). The depicted residues are Tyr70, Leu92, Thr95, and His123, and the amino acids with a polar side chain located within 5 Å from the heme propionates.

Tyr70 does not (*12*). The hydrogen-bonding interaction between Thr95 and the heme-bound $O_2$ would be responsible for selective $O_2$ sensing and intramolecular signal transduction upon $O_2$ binding.

In this study, we characterized the coordination structure of the heme and the hydrogen-bonding pattern on the heme-bound ligands and on the heme propionates in $O_2$-, CO-, and NO-bound forms of the wild type (WT) and several mutants of full-length HemAT-*Bs* to investigate the mechanism of selective $O_2$ sensing by HemAT-*Bs*. On the basis of these results, we show that the formation of a hydrogen bond between His86 and heme propionate 6 upon $O_2$ binding causes a protein conformational change that allows Thr95 to form a specific hydrogen bond to the heme-bound $O_2$.

## EXPERIMENTAL PROCEDURES

In this study, we used full-length HemAT-*Bs* with a *C*-terminal $His_6$-tag, which was expressed in *E. coli* BL21-(DE3) under the control of the T7 promoter in the pET-24-(+) vector (Novagen). Site-directed mutagenesis was carried out using a QuikChange Site-Directed Mutagenesis Kit (Stratagene). For the expression of HemAT-*Bs*, the *E. coli* cells were grown aerobically at 37 °C for 4 h in Terrific Broth containing 30 $\mu$g/mL of kanamycin. The expression was induced by the addition of isopropyl-$\beta$-D-thiogalactopyranoside to a final concentration of 1 mM, and then the cultivation was continued at 22 °C for 18 h. The cells were harvested by centrifugation at 4000*g* and were stored at −78 °C until use.

The cells were thawed and resuspended in buffer A (50 mM Tris-HCl buffer (pH 8.0) containing 15 mM glycine and 1 M NaCl) and then broken by sonication. The resulting suspension was centrifuged at 100 000*g* for 20 min, and the supernatant was loaded on a $Ni^{2+}$-charged HiTrap Chelating column (Amersham Biosciences Corp.). After washing the column with buffer A, and then with 50 mM Tris-HCl buffer (pH 8.0), the adsorbed proteins were eluted by 50 mM Tris-HCl buffer (pH 8.0) containing 100 mM imidazole. The fractions containing HemAT-*Bs* were combined and loaded on a HiTrap Q HP column (Amersham Biosciences Corp.). The column was washed with 50 mM Tris-HCl buffer (pH 8.0) containing 100 mM NaCl, and then HemAT-*Bs* was eluted by increasing the concentration of NaCl in the buffer.

HemAT-*Bs* was oxidized by adding a small amount of potassium ferricyanide. Excess potassium ferricyanide was removed by using a PD10 column (Amersham Biosciences Corp.) with 50 mM Tris-HCl buffer (pH 8.0). Five times excess amount of sodium dithionite was added into degassed ferric HemAT-*Bs* solution to make ferrous HemAT-*Bs*. To prepare CO-, NO-, and $O_2$-bound HemAT-*Bs*, the ferrous HemAT-*Bs* solution was exposed to CO, NO, and $O_2$ gas, respectively.

EPR spectra of NO-bound HemAT-*Bs* were measured at 20 K on a Bruker ESP300E spectrometer with a microwave frequency of 9.5 GHz and a modulation amplitude of 5.0 G.

Resonance Raman spectra of HemAT-*Bs* were measured as reported previously (*12*, *13*). The excitation source was a $Kr^+$ laser (Spectra Physics 2060) at 413.1 and 406.7 nm for the $O_2$- and CO-bound forms and for the NO-bound form, respectively. The scattered light was dispersed with a single polychromator (Ritsu DG-1000) equipped with a liquid nitrogen-cooled charge-coupled device camera. The Raman shifts obtained were calibrated using indene and an aqueous solution of potassium ferrocyanide. The laser power was 0.2 mW for the CO-bound form and 1 mW for the $O_2$- and NO-bound forms at the sample point.

In the resonance Raman spectra of $O_2$-bound HemAT-*Bs*, some isotope ($^{16}O_2$ and $^{18}O_2$)-insensitive bands overlap with the Fe—$O_2$ stretching bands. Gaussian-bands fitting analyses of the resonance Raman spectra of the $O_2$-bound forms were carried out with Igor Pro 5.03 for distinguishing the Fe—$O_2$ modes from other isotope-insensitive modes (*12*). The width, peak position, and intensity ratio for the isotope-insensitive modes were fixed for the fitting of $^{16}O_2$ and $^{18}O_2$ spectra.

## RESULTS

The electronic absorption spectra of the CO-bound form of WT, T95A, and Y70F HemAT-*Bs* showed the Soret, $\beta$, and $\alpha$ peaks at 422, 542, and 566 nm, respectively (Figure S1A, Supporting Information). These spectra are typical of CO-bound heme proteins with a 6-coordinated, low-spin heme. All of the NO-bound form of WT, T95A, and Y70F HemAT-*Bs* gave the same spectra with the Soret, $\beta$, and $\alpha$ peaks at 419, 548, and 575 nm, respectively (Figure S1B, Supporting Information). These spectra are typical of a 6-coordinate, low-spin Fe(II) nitrosyl heme with a proximal histidine ligand, as seen in NO-bound myoglobin (Mb) (*14*).

Figure 2 shows the EPR spectra of NO-bound HemAT-*Bs*. The first derivative spectrum with $g = 2.08$, 2.01, and 1.97 was typical of a 6-coordinated Fe(II) nitrosyl heme (*15*) (Figure 2A). The hyperfine coupling constants derived from the nitrogen atoms of the heme-bound NO and the proximal histidine were determined to be $A_1 = 2.2$ mT and $A_2 = 0.6$ mT, respectively (Figure 2B). The EPR spectra of T95A and Y70F HemAT-*Bs* were the same as that of WT (data not shown). These results indicate the formation of a 6-coordinated nitrosyl heme with a proximal histidine in the NO-

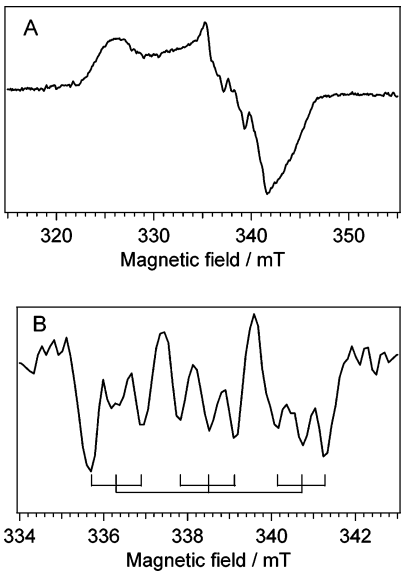


FIGURE 2: (A) First derivative EPR spectrum and the (B) second derivative EPR spectrum of NO-bound WT HemAT-*Bs* in 50 mM Tris-HCl buffer (pH 8.0). These spectra were recorded at 20 K with the microwave frequency at 9.5 GHz and the modulation amplitude at 5.0 G.

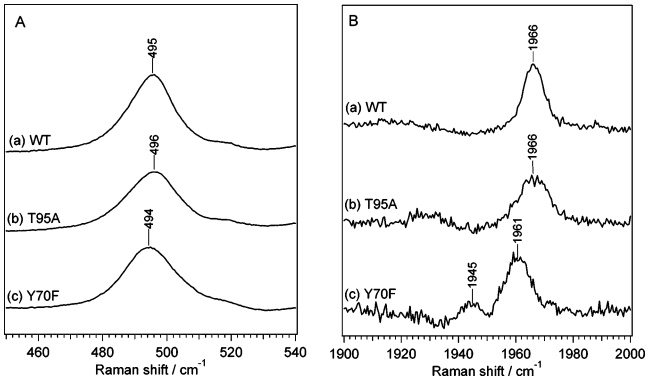


FIGURE 3: Resonance Raman spectra of CO-bound (a) WT, (b) T95A, and (c) Y70F HemAT-*Bs*. (A) Fe−CO stretching bands in the low-frequency region. (B) C−O stretching bands in the high-frequency region.

bound form, which is consistent with the results from electronic absorption spectroscopy.

Fe−C and C−O stretching frequencies of CO-bound heme proteins, $\nu_{Fe-CO}$ and $\nu_{C-O}$, are sensitive and reliable markers for the electrostatic environment around the heme-bound CO (*16*). The $\nu_{Fe-CO}$ and $\nu_{C-O}$ bands of CO-bound WT HemAT-*Bs* were observed at 495 and 1966 $cm^{-1}$, respectively (Figure 3). These values were similar to those of H64I ($\nu_{Fe-CO}$ = 490 $cm^{-1}$, $\nu_{C-O}$ = 1968 $cm^{-1}$) and H64L ($\nu_{Fe-CO}$ = 490 $cm^{-1}$, $\nu_{C-O}$ = 1965 $cm^{-1}$) Mbs (*17*), but different from those of WT Mb ($\nu_{Fe-CO}$ = 512 $cm^{-1}$, $\nu_{C-O}$ = 1944 $cm^{-1}$) (*18*). These results indicate that the heme-bound CO is in a hydrophobic environment without any hydrogen-bonding interaction in WT HemAT- *Bs*.

T95A HemAT-*Bs* gave $\nu_{Fe-CO}$ and $\nu_{C-O}$ values similar to those of WT HemAT-*Bs*, indicating that the environment around the CO in T95A HemAT-*Bs* is also hydrophobic without hydrogen-bonding on the CO and that the mutation of Thr95 makes little effect on the environment around the heme-bound CO. However, Y70F HemAT-*Bs* showed different resonance Raman spectra from those of WT and T95A HemAT-*Bs*. Two $\nu_{C-O}$ bands were observed at 1961 and 1945 $cm^{-1}$ in Y70F HemAT-*Bs* (Figure 3). Furthermore, a weak shoulder around 510 $cm^{-1}$ was observed in the $\nu_{Fe-CO}$ region of Y70F HemAT-*Bs*, which may correlate with the new $\nu_{Fe-CO}$ band observed at 1945 $cm^{-1}$. These results suggest the existence of two conformers of Fe−CO unit with different environments around the heme-bound CO in this mutant.

In the crystal structure of subunit A in the deoxy form of the HemAT-*Bs* sensor domain (*11*), the phenyl oxygen atom of the Tyr70 side chain is just above the heme iron atom with a distance of 5.8 Å. This fact implies that the nonbonding electron pair on the oxygen atom of the phenyl group of Tyr70 would interact with the oxygen atom of the heme-bound CO. The 5 $cm^{-1}$ low-frequency shift seen in the $\nu_{C-O}$ band of Y70F HemAT-*Bs* (the $\nu_{C-O}$ at 1961 $cm^{-1}$) is consistent with the disappearance of this interaction by the mutation. In addition, the oxygen atom of the Tyr70 side chain is close to the carbonyl oxygen atom of Leu92 with a distance of 2.9 Å, which is consistent with the presence of a hydrogen bond between Tyr70 and Leu92 (*11*). The disappearance of this hydrogen bond in the Y70F mutant would cause a considerable conformational perturbation in the distal heme pocket. The new $\nu_{C-O}$ band at 1945 $cm^{-1}$ and the weak shoulder at ca. 510 $cm^{-1}$ seen in this mutant might be caused by this structural perturbation.

Zhang et al. reported that the Tyr70 mutants of the HemAT-*Bs* sensor domain showed large dissociation constants for the heme-bound $O_2$ and proposed that Tyr70 would form a hydrogen bond to the heme-bound $O_2$ on the basis of these results (*6*). Our previous results, however, have shown that Tyr70 does not form such a hydrogen bond in the full-length of HemAT-*Bs* (*12*). Their results imply that Tyr70 is responsible for the fixation of the position of Thr95 that forms the hydrogen bond with the heme-bound $O_2$. Leu92 and Thr95 are located in the same helix, the E-helix. If the hydrogen bond between Leu92 and Tyr70 disappear, the position of the E-helix would be perturbed, resulting in the low stability of the $O_2$-bound form of Tyr70 mutants. In addition, we have also shown that the hydrogen-bonding pattern around the heme-bound $O_2$ is different between the full-length and the truncated sensor domain of HemAT-*Bs* (*12*). These results suggest that the affinity of $O_2$ and the hydrogen-bonding interaction around the heme-bound $O_2$ are different between the truncated sensor domain and the full-length of HemAT-*Bs*.

N−O stretching frequency, $\nu_{N-O}$, of NO-bound heme proteins is also affected by the heme distal environments (*19*). The $\nu_{N-O}$ bands of WT HemAT-*Bs* was observed at 1636 $cm^{-1}$ (Figure 4). This values was similar to that of the $\nu_{N-O}$ of H64L Mb ($\nu_{N-O}$ = 1635 $cm^{-1}$) but not to that of WT Mb ($\nu_{N-O}$ = 1613 $cm^{-1}$) (*19*). These results suggest that the heme-bound NO in WT HemAT-*Bs* is in a hydrophobic environment without any hydrogen bond on the heme-bound NO.

The Fe−NO stretching mode, $\nu_{Fe-NO}$, of NO-bound WT HemAT-*Bs* was observed at 545 $cm^{-1}$ (Figure 4). The $\nu_{Fe-NO}$ band is not sensitive to the electrostatic environment of the distal heme pocket (*19*). Rather, the $\nu_{Fe-NO}$ frequency is reported to be dependent on the Fe−N−O angle (*20*). This frequency is lowered by decreasing the Fe−N−O angle (*20*). The $\nu_{Fe-NO}$ frequency of NO-bound HemAT-*Bs* (545 $cm^{-1}$)

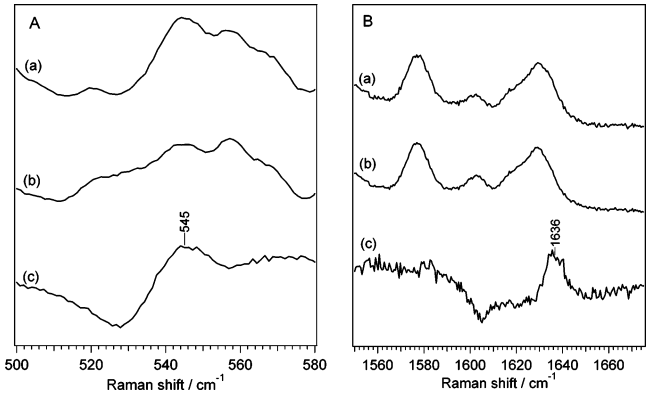


FIGURE 4: Resonance Raman spectra of NO-bound HemAT-*Bs*. (a) $^{14}$NO-bound WT HemAT-*Bs*, (b) $^{15}$NO-bound WT HemAT-*Bs*, and (c) (a)−(b) difference spectrum.

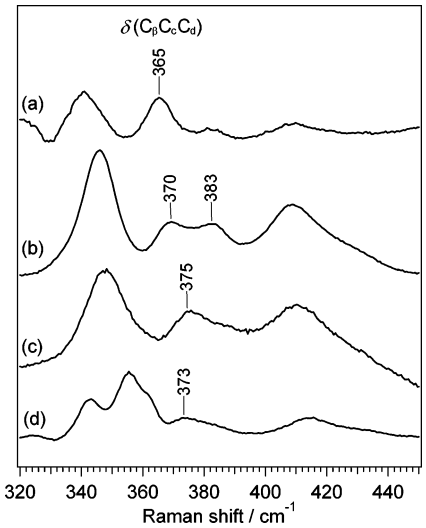


FIGURE 5: Resonance Raman spectra of WT HemAT-*Bs* in the (a) ferrous, (b) $O_2$-bound, (c) NO-bound, and (d) CO-bound forms.

was lower than that of NO-bound Mb (558 cm$^{-1}$ (*19*)), suggesting that the Fe−N−O angle in NO-bound HemAT-*Bs* is lower than that in NO-bound Mb.

The bending mode of the heme propionate, $\delta(C_\beta C_c C_d)$, in the resonance Raman spectra of $O_2$-bound HemAT-*Bs* showed a different feature from those of the ferrous, CO- and NO-bound forms. The resonance Raman spectra of ferrous, CO-, and NO-bound HemAT-*Bs* showed one $\delta(C_\beta C_c C_d)$ band at 365, 373, and 375 cm$^{-1}$, respectively (Figure 5). However, in the $O_2$-bound form, two $\delta(C_\beta C_c C_d)$ bands were observed at 370 and 383 cm$^{-1}$, suggesting that there are two species with different conformations around the heme propionates in $O_2$-bound HemAT-*Bs*.

The $\delta(C_\beta C_c C_d)$ band is sensitive to electrostatic interaction on the heme propionates, for example, hydrogen bonds and salt bridges (*21*). The stronger the electrostatic interaction between the heme propionate and the surrounding residues, the higher the frequency of the $\delta(C_\beta C_c C_d)$ band (*21*). The $\delta(C_\beta C_c C_d)$ band at 365, 373, 375, and 370 cm$^{-1}$ in ferrous, CO-, NO-, and $O_2$-bound HemAT-*Bs*, respectively, are lower than those of the corresponding forms of Mb (371, 377, 378, and 378 cm$^{-1}$ for the ferrous, CO-, NO-, and $O_2$-bound forms, respectively (*19*, *22*−*24*)) in which moderate hydrogen bonds exist on heme propionate 7 (*22*). These results indicate that the conformers showing these $\delta(C_\beta C_c C_d)$ bands

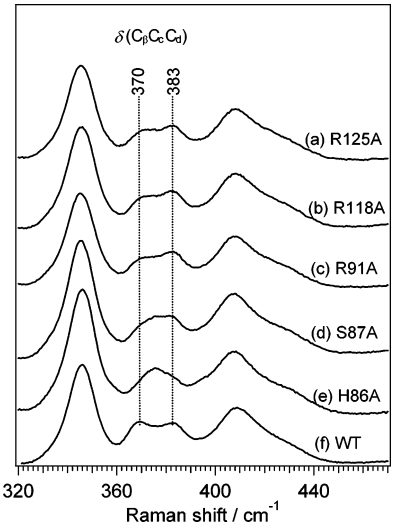


FIGURE 6: Resonance Raman spectra of the $O_2$-bound form of (a) R125A, (b) R118A, (c) R91A, (d) S87A, (e) H86A, and (f) WT HemAT-*Bs*.

have no hydrogen bond or a weak hydrogen bond on the heme propionate.

The additional $\delta(C_\beta C_c C_d)$ band at 383 cm$^{-1}$ in $O_2$-bound HemAT-*Bs* indicates the existence of a stronger hydrogen bond or a salt bridge on the heme propionate. This conformer was observed only in the $O_2$-bound form. To determine the amino acid residues responsible for the 383 cm$^{-1}$ band, we prepared the following five mutants: H86A, S87A, R91A, R118A, and R125A, in which every polar residue within 5 Å from the heme propionates is mutated to alanine (Figure 1). The $\delta(C_\beta C_c C_d)$ band at 383 cm$^{-1}$ disappeared only in $O_2$-bound H86A HemAT-*Bs*, whereas the other mutants (S87A, R91A, R118A, and R125A HemAT-*Bs*) showed almost the same $\delta(C_\beta C_c C_d)$ band at 383 cm$^{-1}$ as WT HemAT-*Bs* did (Figure 6). The 370 cm$^{-1}$ band seen in the spectrum of WT exhibited a 5 cm$^{-1}$ upshift by the mutation of His86 and Ser87, both of which are located in the CE-loop near the heme propionate. This upshift of the 370 cm$^{-1}$ band might be caused by a structural perturbation around the heme propionate. These results indicate that His86 is the residue that forms the hydrogen bond with one of the heme propionates, probably the one at the position 6, and that the residues in the CE-loop are responsible for maintaining the proper structure around the heme propionate.

The Fe—$O_2$ stretching frequency region of the resonance Raman spectrum of H86A HemAT-*Bs* was also different from that of WT HemAT-*Bs*. We previously reported that three $\nu_{Fe-O2}$ bands were observed at 554, 566, and 572 cm$^{-1}$ in $O_2$-bound WT HemAT-*Bs* (*12*). In H86A HemAT-*Bs*, the band at 566 cm$^{-1}$ disappeared, and only the bands at 557 and 572 cm$^{-1}$ were observed as shown in Figure 7. These bands were shifted to 538 and 554 cm$^{-1}$, respectively, upon $^{18}O_2$ substitution. These isotope shifts of 19 and 18 cm$^{-1}$ were consistent with the previously reported values for WT HemAT-*Bs* and were in agreement with a calculated shift value of 21 cm$^{-1}$ (*12*). The $^{16}O_2-^{18}O_2$ difference spectrum was also consistent with the result of the Gaussian fitting analysis (Figure 7C). The difference in the Fe−O−O bond angle affects the shift of the Fe—$O_2$ stretching mode upon isotope substitution of $O_2$, which causes a slight difference between the experimental and calculated values of the isotope

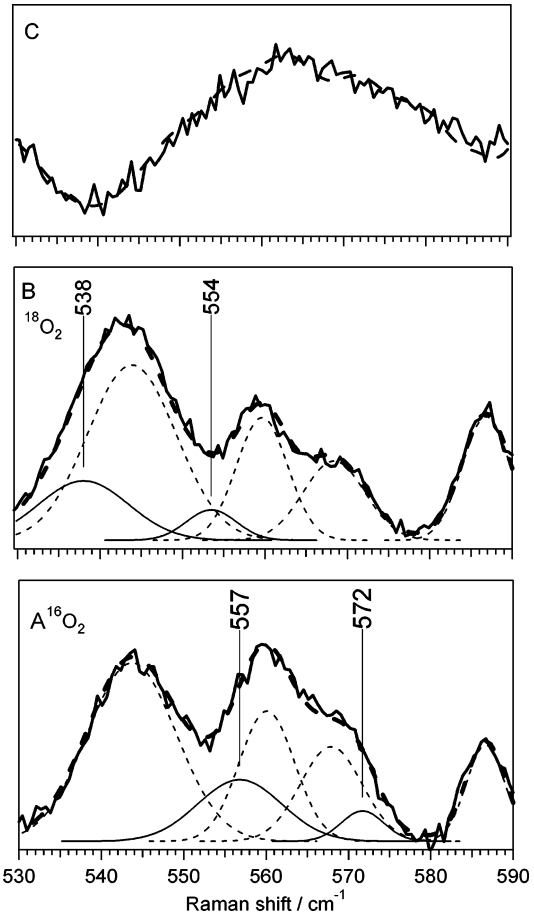


FIGURE 7: Resonance Raman spectra of (A) $^{16}O_2$-bound H86A HemAT-*Bs* and (B) $^{18}O_2$-bound H86A HemAT-*Bs*. The bold solid lines are the raw spectra. All traces except for the bold solid lines were obtained by Gaussian band fitting analysis. The thin solid lines denote the contributions from $\nu_{Fe-O2}$, which were sensitive to the isotope substitution of $O_2$. The thin dotted lines are due to the isotope-insensitive modes. The bold dotted lines are the sum of the component bands. (C) $^{16}O_2-^{18}O_2$ difference spectra. The broken line in the spectrum (C) is the difference spectrum obtained by Gaussian band fitting analysis. The bold solid line is the experimental difference spectrum.

shift. These results indicate that the loss of the hydrogen bond between His86 and heme propionate 6 affects the hydrogen-bonding interaction between the heme-bound $O_2$ and Thr95.

## DISCUSSION

It is a critical requirement for heme-based gas sensor proteins to discriminate between the effector gas molecule and other gas molecules. Some heme-based gas sensor proteins, such as CooA and sGC, alter the coordination number (5-coordinate vs 6-coordinate) of the heme depending on the species of heme-bound gas molecules (*25*−*27*). The proper coordination structure with the effector molecule causes a protein conformational change that is essential to a specific response to the cognate effectors. The heme of HemAT-*Bs*, however, has a 6-coordinate structure in all of the $O_2$-, CO-, and NO-bound forms, indicating that HemAT-*Bs* does not adopt this strategy for selective $O_2$ sensing.

Another possible strategy for heme-based gas sensor proteins to discriminate the effector gas molecule is to form a specific interaction between the heme-bound effector molecule and neighboring amino acid residues. We have reported that Thr95 forms the hydrogen bonds to the heme-bound $O_2$ in the two conformers among the three in the $O_2$-bound form (*12*). However, we have revealed here that no hydrogen bond is formed on the heme-bound ligand in the case of CO- and NO-bound HemAT-*Bs*. These results show that hydrogen bonding between a heme-bound ligand and Thr95 is specific in the $O_2$-bound form, which supports the idea that this hydrogen-bonding interaction is essential for selective $O_2$ sensing by HemAT-*Bs*.

The crystal structure of the HemAT-*Bs* sensor domain in the ferrous form shows that the distances between the hydroxyl oxygen atom of Thr95 and the heme iron atom are 6.8 and 7.6 Å in subunits A and B, respectively (*11*). To form the direct hydrogen bond to the heme-bound $O_2$, Thr95 has to be located within 3 Å from the heme iron. Although the above distances in the ferrous form are too long to form a hydrogen bond, a direct hydrogen bond is certainly formed between Thr95 and the proximal oxygen atom of the heme-bound $O_2$ (*12*). These results indicate that the formation of the hydrogen bond between Thr95 and the proximal oxygen atom requires a preceding conformational change of the distal heme pocket that moves Thr95 to the suitable position to form the hydrogen bond.

Because the $O_2$-bound H86A HemAT-*Bs* cannot form the conformer with the direct hydrogen bond between Thr95 and the proximal oxygen atom, the preceding conformational alteration would be induced by the formation of the hydrogen bond between His86 and heme propionate 6, as discussed below. His86 is located in the CE-loop, which is adjacent to the E-helix that contains Thr95. The formation of the hydrogen bond between His86 and heme propionate 6, which takes place only upon $O_2$ binding, will induce a conformational change of the CE-loop. Then, this conformational alteration of the CE-loop will propagate to the E-helix, finally shifting Thr95 to the proper position to form the direct hydrogen bond to the proximal oxygen atom. Thus, HemAT-

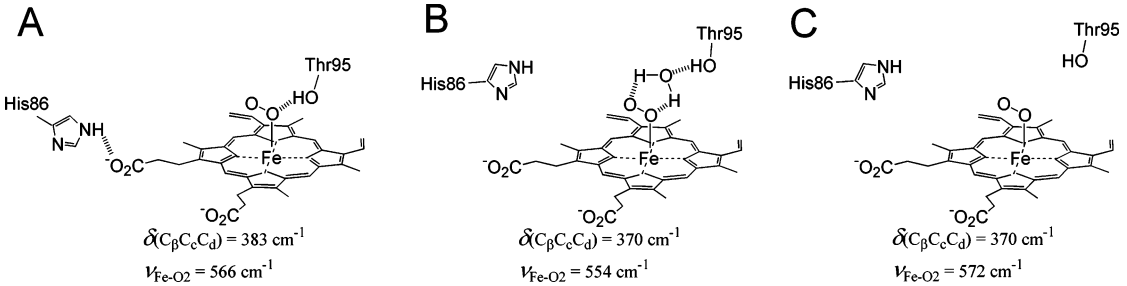


FIGURE 8: Proposed model of the heme environmental structure with different hydrogen-bonding interactions in $O_2$-bound HemAT-*Bs*. The hashed lines indicate hydrogen bonds.

*Bs* would cause a stepwise conformational change upon $O_2$ binding.

If Thr95 were located in advance at the suitable position to form the hydrogen bond to the heme-bound $O_2$ in ferrous form, Thr95 would also form a similar hydrogen bond to the heme-bound CO and NO. In this situation, the hydrogen bond between Thr95 and the heme-bound $O_2$ could not be used for selective $O_2$ sensing. The stepwise conformational change upon $O_2$ binding allows the hydrogen bond between Thr95 and the heme-bound ligand to be specific for the $O_2$-bound form.

On the basis of these results, we propose the heme environmental structure of $O_2$-bound HemAT-*Bs* shown in Figure 8. Three conformers exist in $O_2$-bound HemAT-*Bs* with different hydrogen-bonding interactions on the heme-bound $O_2$, corresponding to the closed, open α, and open $\beta$ forms (*12*). The hydrogen-bonding interaction on the heme propionate is also different in these three conformers. His86 forms the hydrogen bond to the heme propionate in the open α form in which the direct hydrogen bond is formed between Thr95 and heme-bound $O_2$. His86 does not form the hydrogen bond with the heme propionate in the closed and open $\beta$ forms in which Thr95 does not come close to the heme-bound $O_2$.

HemAT-*Bs* should undergo a sufficient conformational change upon $O_2$ binding for generating the aerotactic signal. The formation of the open α form involves a considerable conformational change of the CE-loop and the E-helix, suggesting that the open α form is the on-state for the signaling. In the closed and open $\beta$ forms, the conformational change of the CE-loop and the E-helix will not be so large because the hydrogen bond is not formed between His86 and the heme propionate. Therefore, the closed and the open $\beta$ forms will be the off-state. It remains to be elucidated why the on- and off-states exist together in $O_2$-bound HemAT-*Bs*, and whether the closed and open $\beta$ forms have any physiological role.

In summary, we propose the following mechanism for selective $O_2$ sensing and signal transduction in HemAT-*Bs*. When $O_2$ is bound to the heme in HemAT-*Bs*, the hydrogen bond forms between His86 and heme propionate 6. The formation of this hydrogen bond makes a conformational alteration in the distal heme pocket, especially on the position of the E-helix. The change in the position of the E-helix makes Thr95 be located at the suitable position to form the hydrogen bond with the proximal oxygen atom of the heme-bound $O_2$. As the hydrogen bond is not formed between His86 and heme propionate 6 upon CO and NO binding, the proper conformational change does not occur in these cases. The proper conformational change around the heme upon $O_2$ binding will propagate to the signaling domain of HemAT-*Bs*, and then activate CheA.

## SUPPORTING INFORMATION AVAILABLE

Electronic absorption spectra of CO- and NO-bound HemAT-*Bs* and the details of the Gaussian-fit analysis of the resonance Raman spectra of $O_2$-bound H86A HemAT-*Bs*. This material is available free of charge via the Internet at http://pubs.acs.org.

## REFERENCES

1. Rodgers, K. R. (1999) Heme-based sensors in biological systems, *Curr. Opin. Chem. Biol. 3*, 158−167.
2. Chan, M. K. (2001) Recent advances in heme-protein sensors, *Curr. Opin. Chem. Biol. 5*, 216−222.
3. Jain, R., and Chan, M. K. (2003) Mechanisms of ligand discrimination by heme proteins, *J. Biol. Inorg. Chem. 8*, 1−11.
4. Hou, S., Larsen, R. W., Boudko, F., Riley, C. W., Karatan, E., Zimmer, M., Ordal, G. W., and Alam, M. (2000) Myoglobin-like aerotaxis transducers in Archaea and Bacteria, *Nature 403*, 540−544.
5. Aono, S., Kato, T., Matsuki, M., Nakajima, H., Ohta, T., Uchida, T., and Kitagawa, T., (2002) Resonance Raman and ligand binding studies of the oxygen-sensing signal transducer protein HemAT from *Bacillus subtilis*, *J. Biol. Chem. 277*, 13528−13538.
6. Zhang, W., Olson, J. S., and Phillips, G. N., Jr. (2005) Biophysical and kinetic characterization of HemAT, an aerotaxis receptor from *Bacillus subtilis*, *Biophys. J. 88*, 2801−2814.
7. Ohta, T., and Kitagawa, T. (2005) Resonance Raman investigation of the specific sensing mechanism of a target molecule by gas sensory proteins, *Inorg. Chem. 44*, 758−769.
8. Szurmant, H., and Ordal, G. W. (2004) Diversity in chemotaxis mechanisms among the bacteria and archaea, *Microbiol. Mol. Biol. Rev. 68*, 301−319.
9. Bischoff, D. S., and Ordal, G. W (1992) *Bacillus subtilis* chemotaxis: a deviation from the *Escherichia coli* paradigm, *Mol. Microbiol. 6*, 23−28.
10. Garrity, L. F., and Ordal G, W. (1995) Chemotaxis in *Bacillus subtilis*: how bacteria monitor environmental signals, *Pharmacol. Ther. 68*, 87−104.
11. Zhang, W., and Phillips, G. N., Jr. (2003) Structure of the oxygen sensor in *Bacillus subtilis*: signal transduction of chemotaxis by control of symmetry, *Structure 11*, 1097−1110.
12. Ohta, T., Yoshimura, H., Yoshioka, S., Aono, S., and Kitagawa, T. (2004) Oxygen-sensing mechanism of HemAT from *Bacillus subtilis*: A resonance Raman spectroscopic study, *J. Am. Chem. Soc. 126*, 15000−15001.
13. Aono, S., Nakajima, H., Ohta, T., and Kitagawa, T. (2004) Resonance Raman and ligand-binding analysis of the oxygen-sensing signal transducer protein HemAT from *Bacillus subtilis*, *Methods Enzymol. 381*, 618−628.
14. Yoshimura, T., and Ozaki, T. (1984) Electronic-spectra for nitrosyl-(protoporphyrin-IX dimethyl ester)iron(II) and its complexes with nitrogenous bases as model systems for nitrosylhemoproteins, *Arch. Biochem. Biophys. 229*, 126−135.
15. Yoshimura, T., Ozaki, T., Shintani, Y., and Watanabe, H. (1979) Electron-paramagnetic resonance of nitrosylprotoheme dimethyl ester complexes with imidazole derivatives as model systems for nitrosylhemoproteins, *Arch. Biochem. Biophys. 193*, 301−313.
16. Spiro, T. G., and Wasbotten, I. H. (2005) CO as a vibrational probe of heme protein active site, *J. Inorg. Biochem. 99*, 34−44.
17. Li, T. S., Quillin, M. L., Phillips G. N., Jr., and Olson, J. S. (1994) Structural determinants of the stretching frequency of CO bound to myoglobin, *Biochemistry 33*, 1433−1446.
18. Tsubaki, M., Srivastava, R. B., and Yu, N. T. (1982) Resonance Raman investigation of carbon monoxide bonding in (carbon monoxy) hemoglobin and -myoglobin: detection of iron−carbon monoxide stretching and iron−carbon−oxygen bending vibrations and influence of the quaternary structure change, *Biochemistry 21*, 1132−1140.
19. Tomita, T., Hirota, S., Ogura, T., Olson, J. S., and Kitagawa, T. (1999) Resonance Raman investigation of Fe−N−O structure of nitrosylheme in myoglobin and its mutants, *J. Phys. Chem. B 103*, 7044−7054.
20. Hu, S., and Kincaid, J. R. (1991) Resonance Raman characterization of nitric oxide adducts of cytochrome P450cam: the effect of substrate structure on the iron-ligand vibrations, *J. Am. Chem. Soc. 113*, 2843−2850.
21. Uchida, T., and Kitagawa, T. (2005) Mechanism for transduction of the ligand-binding signal in heme-based gas sensory proteins revealed by resonance Raman spectroscopy, *Acc. Chem. Res. 38*, 662−670.
22. Peterson, E. S., Friedman, J. M., Chien, E. Y. T., and Sligar, S. G. (1998) Functional implications of the proximal hydrogen-bonding network in myoglobin: a resonance Raman and kinetic study of Leu89, Ser92, His97, and F-helix swap mutants, *Biochemistry 37*, 12301−12319.
23. Hirota, S., Ogura, T., Shinzawa-Itoh, K., Yoshikawa, S., Nagai, M., and Kitagawa, T. (1994) Vibrational assignments of the FeCO unit of CO-bound heme proteins revisited: Observation of a new CO-isotope-sensitive Raman band assignable to the FeCO bending fundamental, *J. Phys. Chem. 98*, 6652−6660.

24. Hirota, S., Ogura, T., Appelman, E. H., Shinzawa-Itoh, K., Yoshikawa, S., and Kitagawa, T. (1994) Observation of a new oxygen-isotope sensitive Raman band for oxyhemoproteins and its implications in heme pocket structures, *J. Am. Chem. Soc. 116*, 10564−10570.
25. Traylor, T. G., and Sharma, V. S. (1992) Why NO?, *Biochemistry 31*, 2847−2849.
26. Russwurm, M., and Koesling, D. (2004) NO activation of guanylyl cyclase, *EMBO J. 23*, 4443−4450.
27. Aono, S. (2003) Biochemical and biophysical properties of the CO-sensing transcriptional activator CooA, *Acc. Chem. Res. 36*, 825−831.

BI060315C